

Article

Lignin as a Bio-Sourced Secondary Template for ZSM-5 Zeolite Synthesis

Camila Gomes Flores ^{1,*} , Helena Schneider ²  and Benoit Louis ¹

¹ Institut de Chimie et Procédés pour l’Energie, l’Environnement et la Santé (ICPEES) UMR 7515 du CNRS—Université de Strasbourg, 25 Rue Becquerel, CEDEX 2, 67087 Strasbourg, France; blouis@unistra.fr

² Chemical Engineering Department, Federal University of Rio Grande do Sul, 2777, Ramiro Barcelos, Porto Alegre 90035-007, Brazil; helenasch@gmail.com

* Correspondence: gomesflores@unistra.fr

Abstract: The aim of this study was to investigate the effect of the addition of lignin as a sacrificial agent in ZSM-5 zeolite synthesis. Peculiar growths of ZSM-5 crystals leading to various textural properties were observed. Hence, the behavior in acid-catalyzed conversion of methanol into hydrocarbons (MTH) shifted from high selectivity toward olefins (>55%) to the sole formation of dimethyl ether (DME). Lignin acted as a bio-sourced secondary template (BSST), impacting the zeolite crystals’ shape and, thus, their physicochemical properties.

Keywords: ZSM-5; lignin; BSST; MTH



Citation: Flores, C.G.; Schneider, H.; Louis, B. Lignin as a Bio-Sourced Secondary Template for ZSM-5 Zeolite Synthesis. *Catalysts* **2022**, *12*, 368. <https://doi.org/10.3390/catal12040368>

Academic Editor: Antonio Eduardo Palomares

Received: 2 March 2022

Accepted: 21 March 2022

Published: 24 March 2022

Publisher’s Note: MDPI stays neutral with regard to jurisdictional claims in published maps and institutional affiliations.



Copyright: © 2022 by the authors. Licensee MDPI, Basel, Switzerland. This article is an open access article distributed under the terms and conditions of the Creative Commons Attribution (CC BY) license (<https://creativecommons.org/licenses/by/4.0/>).

1. Introduction

Zeolites are crystalline aluminosilicates that are known for their well-defined pores and channels. Due to their unique properties, such as pore size, acidity, surface area, and shape selectivity, zeolites are widely used in industry. For instance, they can be used as adsorbents [1,2], ion exchangers [3], fertilizers [4,5], and catalysts [6–9]. The zeolite structures applied in catalytic industrial processes are Y (FAU), beta (BEA), ZSM-5 (MFI), mordenite (MOR), and ferrierite (FER), commonly known as the “big five” [10]. The use of a specific type depends on each zeolite’s individual properties [11]. These include high cost and environmental issues associated with the organic structure-directing agents (OSDAs). Additionally, the extended period required for synthesis and the reproducibility of the synthesis process should be optimized [10].

Among zeolites, MFI materials have several attractive properties, such as low deactivation by coke deposition, high performance in isomerization, and cracking reactions due to the presence of strong acid sites [12,13]. ZSM-5 topology is formed by unit cells consisting of ten-membered rings of T atoms (T = Al or Si) bonded by chain-like oxygen atoms, thus forming channels in a three-dimensional framework [12]. ZSM-5 also exhibits a high silicon-to-aluminum ratio (Si/Al > 10) [12], which improves its physicochemical properties [14–16]. Essentially, increasing the Si/Al ratio decreases Al content and, consequently, the number of acid sites [17].

Zeolites are thermodynamically metastable materials, meaning that initial kinetically formed phases may dissolve and further serve as nutrients to produce denser thermodynamically stable phases. It is possible to inhibit these transformations by proper selection of OSDAs or by interrupting the crystallization toward the targeted structure [18]. Hence, ZSM-5 preparation in academic research usually involves OSDAs. These organic molecules, mainly ammonium ions or amines, self-assemble via electrostatic forces, along with Si and Al tetrahedra, and enable the formation of zeolites with high Si/Al ratios [19]. Usually, OSDAs used for ZSM-5 synthesis are tetrapropylammonium salts [20] or N-butylamine [21]. Despite their advantages, OSDAs remain expensive chemicals, and they are also toxic [22]. Moreover, during their removal upon calcination, the zeolite structure may be damaged [23],

resulting in a release of harmful and polluting gases (i.e., NO_x and CO_2) [22]. Therefore, there are economic and environmental advantages to avoiding the use of organic templates, namely, template-free zeolite synthesis. Template-free crystallization, however, is greatly influenced by the molar composition of the ingredients in the synthesis gel, as well as synthesis duration and temperature [24,25].

A compromise could be found by drastically minimizing the organic template content in the synthesis. Recently, our group proposed an alternative strategy that relied on biomass as a green bio-sourced secondary template (BSST) [26–31]. In these studies, sugar cane bagasse and its derivatives were able to modify the self-assembly of zeolite crystals, yielding different morphological and textural properties. Highly crystalline ZSM-5 was also obtained without OSDAs using rice straw [32], after six days of synthesis.

Hence, the aim of this study was to design new ZSM-5 zeolite families using lignin as a BSST and to investigate the effects of synthesis duration on crystallinity and structural properties. The use of biomass as a sacrificial agent was expected to allow for a significant decrease in tetrapropylammonium hydroxide (TPAOH) concentration. In addition, we expected to form ZSM-5 zeolite crystals with different morphologies and physicochemical properties. The activity of the catalyst was evaluated in the methanol-to-hydrocarbons conversion reaction (MTH).

2. Results and Discussion

ZSM-5 Prepared Using Lignin as BSST

The XRD patterns of ZSM-5 zeolites synthesized at different times (12 h to 24 h) using TPAOH and lignin are displayed in Figures 1 and 2, respectively. The characteristic peaks of the MFI framework ($2\theta = 7.8, 8.7, 23.1, 23.8,$ and 24.3° [33]) were detected in all the conventional ZSM-5 syntheses. No peaks related to other phases (impurities) could be detected.

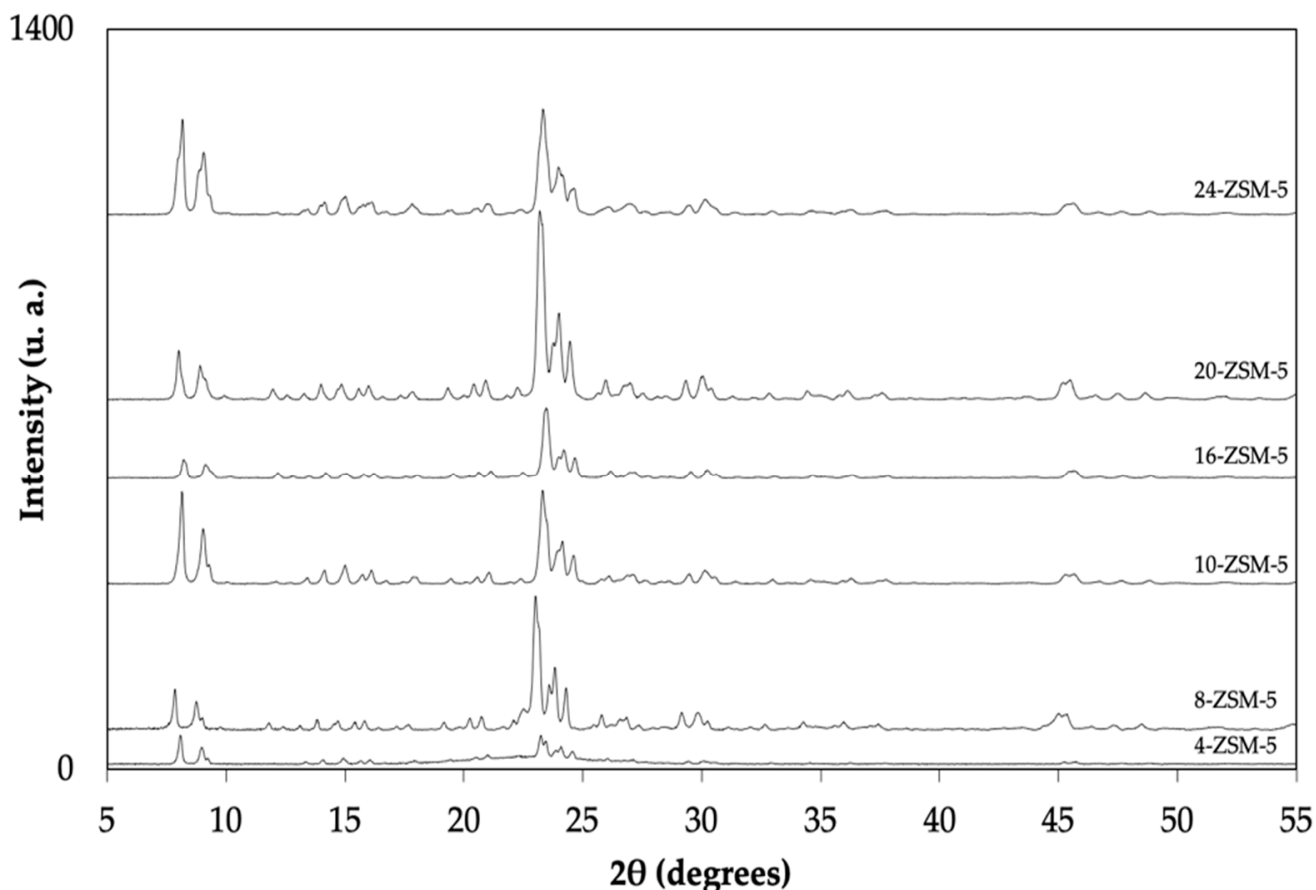


Figure 1. XRD patterns for the ZSM-5 that were synthesized using TPAOH.

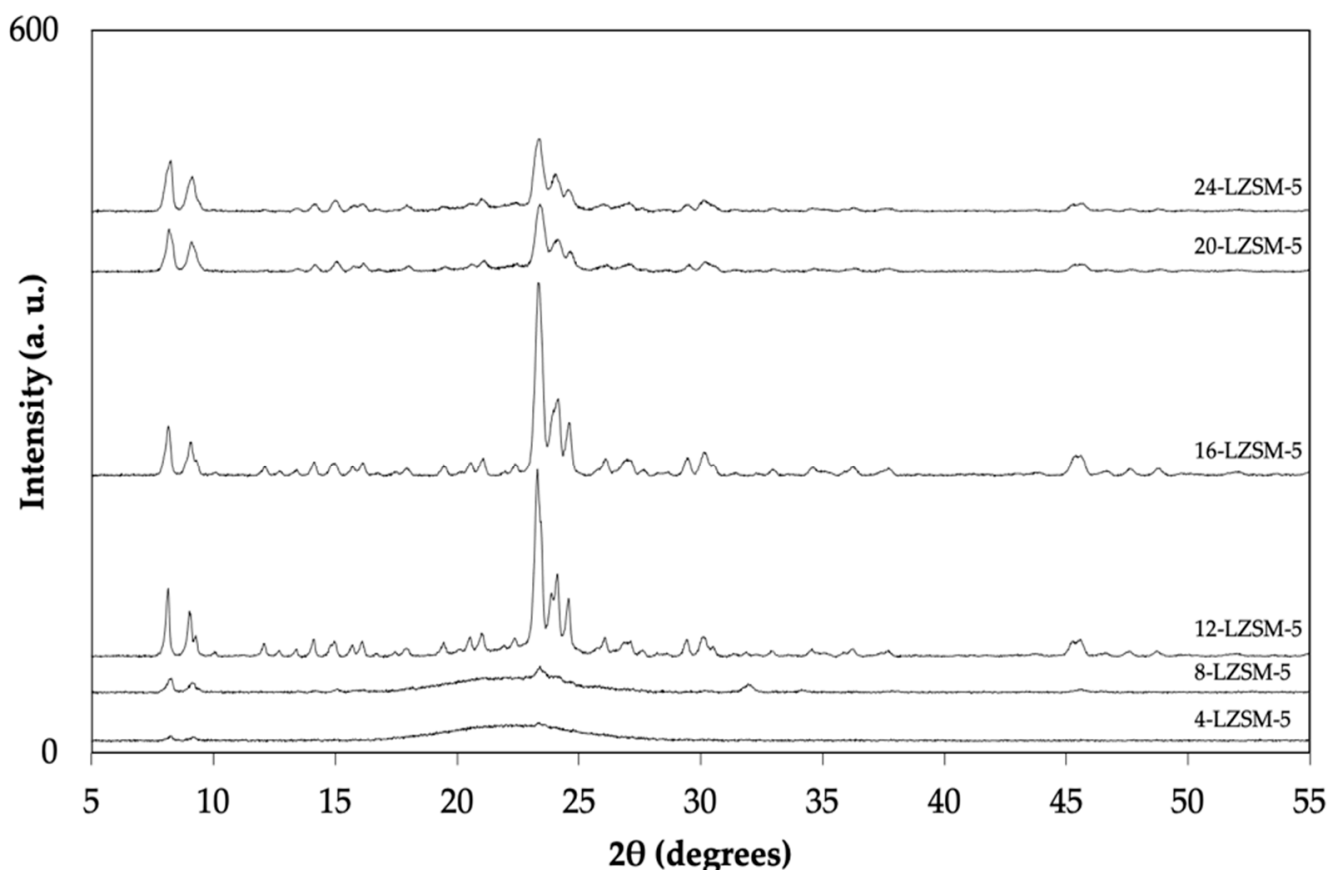


Figure 2. XRD patterns of the ZSM-5 synthesized using lignin.

According to the classical route for ZSM-5 crystallization (using TPAOH solely), a synthesis gel is initially established, and nucleation centers are formed in the pre-aging step. In the case of the shortest synthesis time, 4-ZSM-5, small characteristic peaks from the MFI structure suggested that the primary precursors dissolved in the alkaline solution and began crystallization. After 8 h of hydrothermal synthesis, the characteristic peaks of the MFI zeolite clearly appeared. The highest crystallinity was obtained after 24 h.

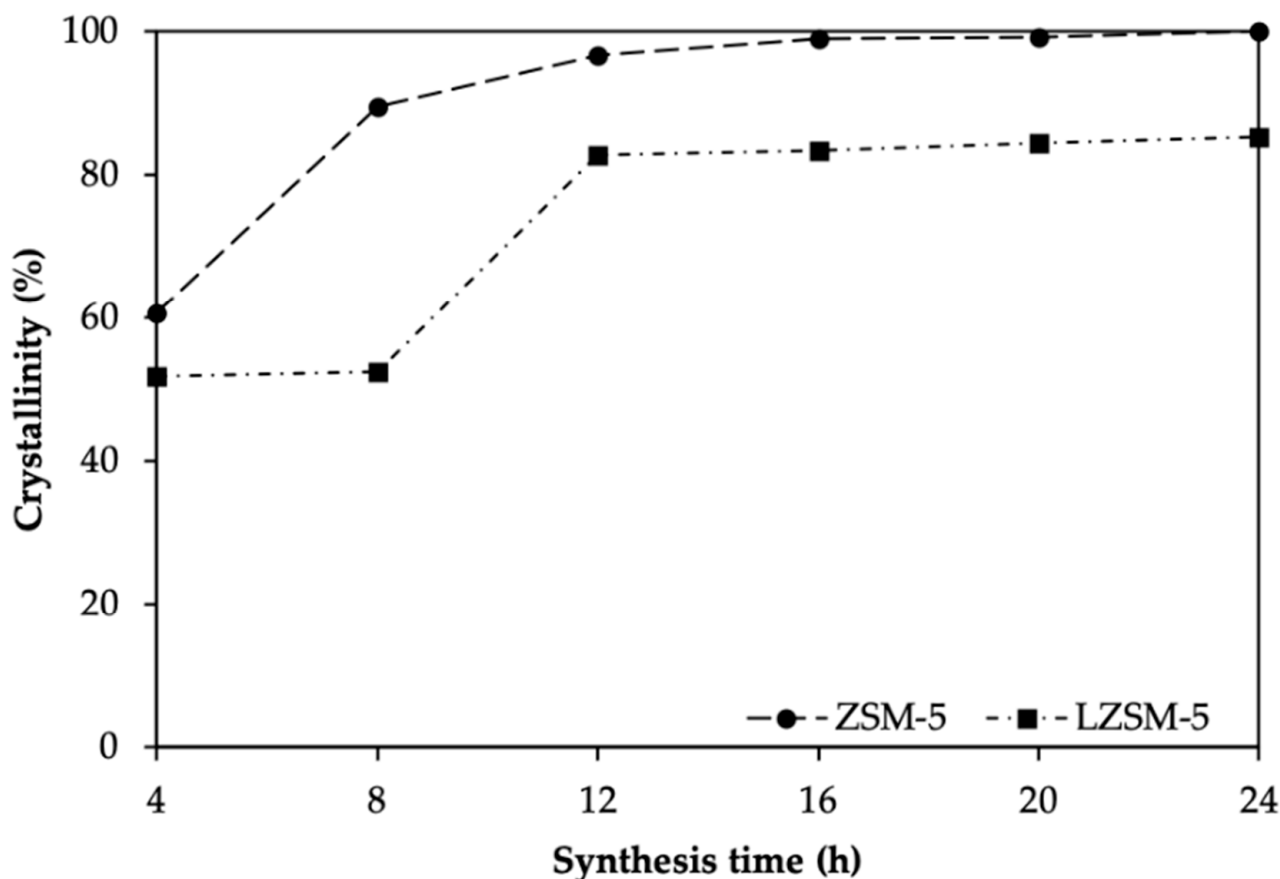
The LZSM-5 samples, synthesized with 50% TPAOH and 50% lignin, exhibited different crystallization kinetics. The use of lignin required a longer time to start zeolite crystallization. As observed in Figure 2, clear diffraction peaks of the MFI structure appeared after 12 h. This might be correlated to the decrease in concentration of the total mineralizing agent (OH^-) added to the gel. Hydroxide is important for kinetic dissolution and polymerization of silica [34,35]. According to Zhang and co-workers [36,37], lignin can either induce a disorder in the crystalline structure of the zeolite or promote redeposition of the crystal subunits.

Relative crystallinity data for ZSM-5 and LZSM-5 samples are listed in Table 1 and represented in Figure 3. For both zeolites, the data suggest that, first, amorphous materials were generated, subsequently developing into crystals through solid–solid transformations. This is similar to what has already been suggested by Grieken and co-workers [38]. ZSM-5 and LZSM-5 achieved the highest relative crystallinity after different synthesis durations. ZSM-5 showed the highest relative crystallinity at 24 h (chosen, therefore as a reference, 100%), whilst LZSM-5 achieved it after 24 h (85%). This could indicate that lignin inhibits ZSM-5 crystal growth, leading to lower crystallization. This result is consistent with the mechanism that is suggested by Louis and co-workers [39].

Table 1. Textural properties (BET specific surface area, total pore volume, microporous volume, and mesoporous volume) and relative crystallinity for all as-synthesized zeolites.

| Sample | $S_{\text{BET}}^{\text{a}}$ ($\text{m}^2 \text{g}^{-1}$) | $V_{\text{total}}^{\text{b}}$ ($\text{cm}^3 \text{g}^{-1}$) | $V_{\text{micro}}^{\text{c}}$ ($\text{cm}^3 \text{g}^{-1}$) | Relative Crystallinity ^d (%) |
|-----------|---|--|--|---|
| 4-ZSM-5 | 192 | 0.917 | 0.012 | 61 |
| 8-ZSM-5 | 143 | 0.098 | 0.044 | 90 |
| 12-ZSM-5 | 357 | 0.207 | 0.115 | 97 |
| 16-ZSM-5 | 387 | 0.211 | 0.123 | 99 |
| 20-ZSM-5 | 368 | 0.192 | 0.114 | 99 |
| 24-ZSM-5 | 348 | 0.184 | 0.110 | 100 |
| 4-LZSM-5 | 46 | 0.050 | 0.009 | 52 |
| 8-LZSM-5 | 86 | 0.450 | 0.004 | 53 |
| 12-LZSM-5 | 197 | 0.110 | 0.060 | 83 |
| 16-LZSM-5 | 318 | 0.180 | 0.102 | 77 |
| 20-LZSM-5 | 352 | 0.120 | 0.052 | 85 |
| 24-LZSM-5 | 334 | 0.110 | 0.052 | 85 |

^a Determined from the multipoint BET method; ^b determined from the adsorbed volume at $P/P_0 = 0.99$; ^c determined from the t-plot method; ^d calculated based on New Eva Software.

**Figure 3.** Relative crystallinity for ZSM-5 and LZSM-5 zeolites.

The textural properties of the catalysts are also listed in Table 1. As crystallinity increased, the specific surface area (S_{BET}) also increased. As previously proposed, the S_{BET} is linked to zeolite crystallinity [40,41].

LZSM-5 catalyst porosity did not present significant changes when compared to ZSM-5. All crystalline LZSM-5 samples exhibited N_2 adsorption isotherms of type IV with a hysteresis loop (Supplementary Materials), indicating the presence of micro- and meso-pores, according to IUPAC classification [42].

ZSM-5 synthesized with only TPAOH also showed isotherms with a hysteresis loop when the synthesis was carried out for less than 12 h (Supplementary Materials). This is related to the initial mesoporous amorphous solid formation, as confirmed by the low relative crystallinity, and is in line with earlier reports [38]. However, zeolites synthesized for over 20 h exhibited a type I isotherm, characteristic of a purely microporous material [42].

The impact of replacing TPAOH with lignin on zeolite morphology was further investigated using SEM (Figure 4). The mapping of Si and Al elements was performed using EDX coupled with SEM, and the same Si/Al ratio was detected in all the samples (26 ± 2). Although lignin maintained crystal homogeneity, two different morphologies for LZSM-5 were observed. This suggests that lignin plays a role in zeolite crystallization. The observed morphologies were coffin-shaped (Figure 4c) and nano-French fries, which agglomerated to form micro-sized spheres (Figure 4d). These ZSM-5 morphologies were also produced by Louis et al. while using sugar cane bagasse as a BSST [29,31,39]. Using new materials as a co-template can indeed reshape the classic zeolite crystal morphology into unusual shapes, leading to zeolites with different properties [26].

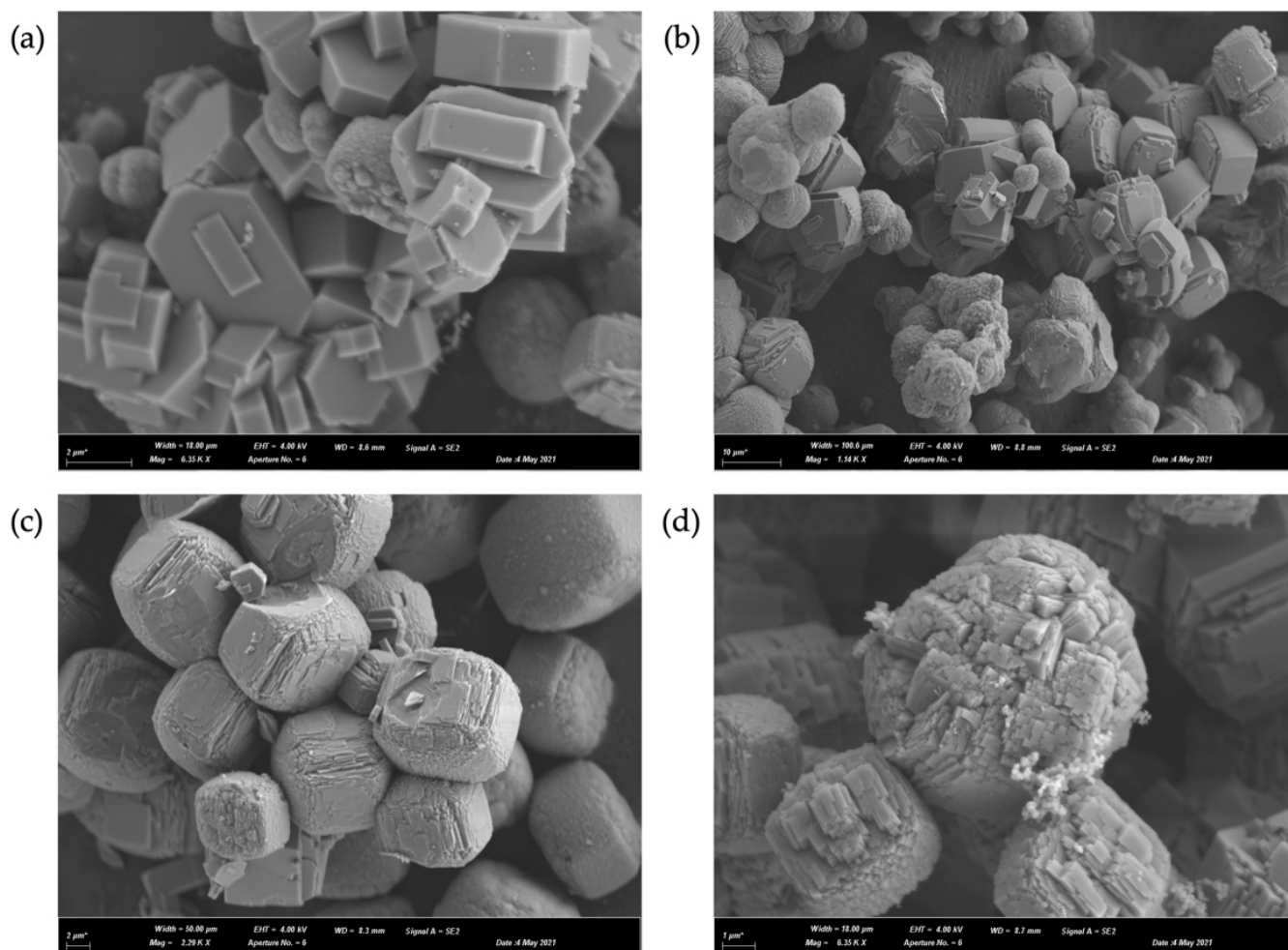


Figure 4. SEM images of 16-ZSM-5 (6350 \times) (a), 16-LZSM-5 (1140 \times) (b), 24-ZSM-5 (2290 \times) (c), and 24-LZSM-5 (6350 \times) (d).

TGA profiles of ZSM-5 synthesized with TPAOH and lignin are shown in Figure 5a. The total weight loss of ZSM-5 using organic TPAOH (8%) is less than that using lignin (10%). This indicates that some lignin residues were embedded within the MFI framework, potentially participating in zeolite crystal growth and acting as a co-template for ZSM-5 framework assembly. This also suggests that alcohols that form the lignin polymer, such

as *p*-coumaryl, coniferyl, and sinapyl [43], may undergo alkoxylation reactions, being anchored to the protozeolitic surface. This may explain the slow crystallinity rate.

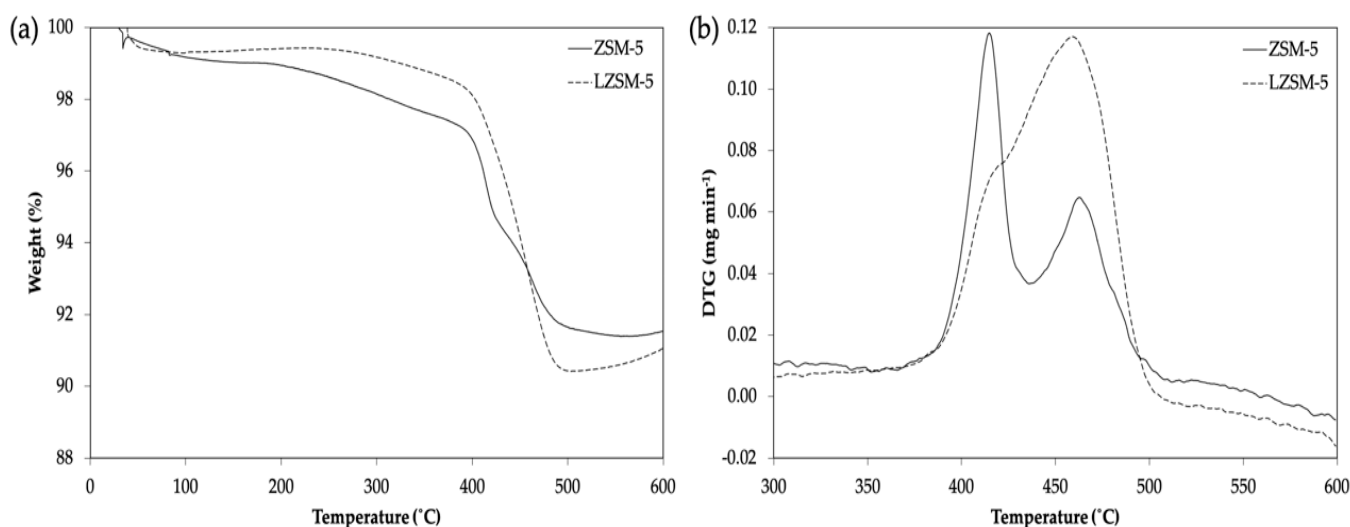


Figure 5. TGA (a) and DTG (b) profiles for ZSM-5 and LZSM-5 synthesized after 24 h.

In comparison, the use of alcohols (methanol, ethanol, 2-propanol, and n-butanol) as solvents that aid the integration of the seed silanization agent on pre-crystallized zeolites generated hierarchical ZSM-5, according to previous studies [44,45]. The authors proposed that the alcohols underwent alkoxylation and were anchored to the protozeolitic units. A similar mechanism was expected to occur using lignin as the BSST.

The weight loss below 200 °C was related to the evaporation of water physisorbed inside the zeolite pores [46]. From 300 to 600 °C, the weight loss was assigned to the decomposition of organic compounds, either TPAOH or lignin [47–49]. Above 550 °C, weight loss may be linked to the combustion of carbonaceous residues formed from the organic degradation and dehydrogenation processes, or to the aromatic ring decomposition present in the lignin [50]. TPA⁺ stabilization around the silicon source might have caused a delay in its decomposition around 330 °C [51].

Lignin degradation usually occurs between 200 and 500 °C [48]. In the current study, lignin decomposition only occurred at temperatures higher than 330 °C, as observed in the DTG profile (Figure 5b), suggesting that lignin was strongly bonded to the ZSM-5 framework. The peaks observed in the DTG profile of L-ZSM-5 (Figure 5b) are most likely related to the breaking of β -O-4, C-C, and β - β bonds during lignin decomposition [49,52].

Even though the samples exhibited the same Si/Al ratio, their acidic properties were also investigated. 20-ZSM-5 and 20-LZSM-5 were evaluated by temperature-programmed desorption of ammonia (NH₃-TPD), as shown in Figure 6. This analysis provided information about the number of acid sites, as well as their strength [53].

As shown in Figure 6, the zeolites displayed a similar TPD profile with two desorption peaks. The dominant peak around 285–295 °C corresponds to mild acid sites, and the second broader peak in the range of 400–600 °C encompasses medium and strong acid sites [54,55]. The strongest acid sites are related to Brønsted acid sites [56].

Table 2 presents the quantities of acid sites based on the amount of NH₃ adsorbed, calculated from the area of the peaks. Interestingly, the second desorption peak (from strong and medium acid sites) was more pronounced for ZSM-5 than for LZSM-5. This indicates the presence of more strong acid sites in ZSM-5 (0.70 mmol g⁻¹) than in LZSM-5.

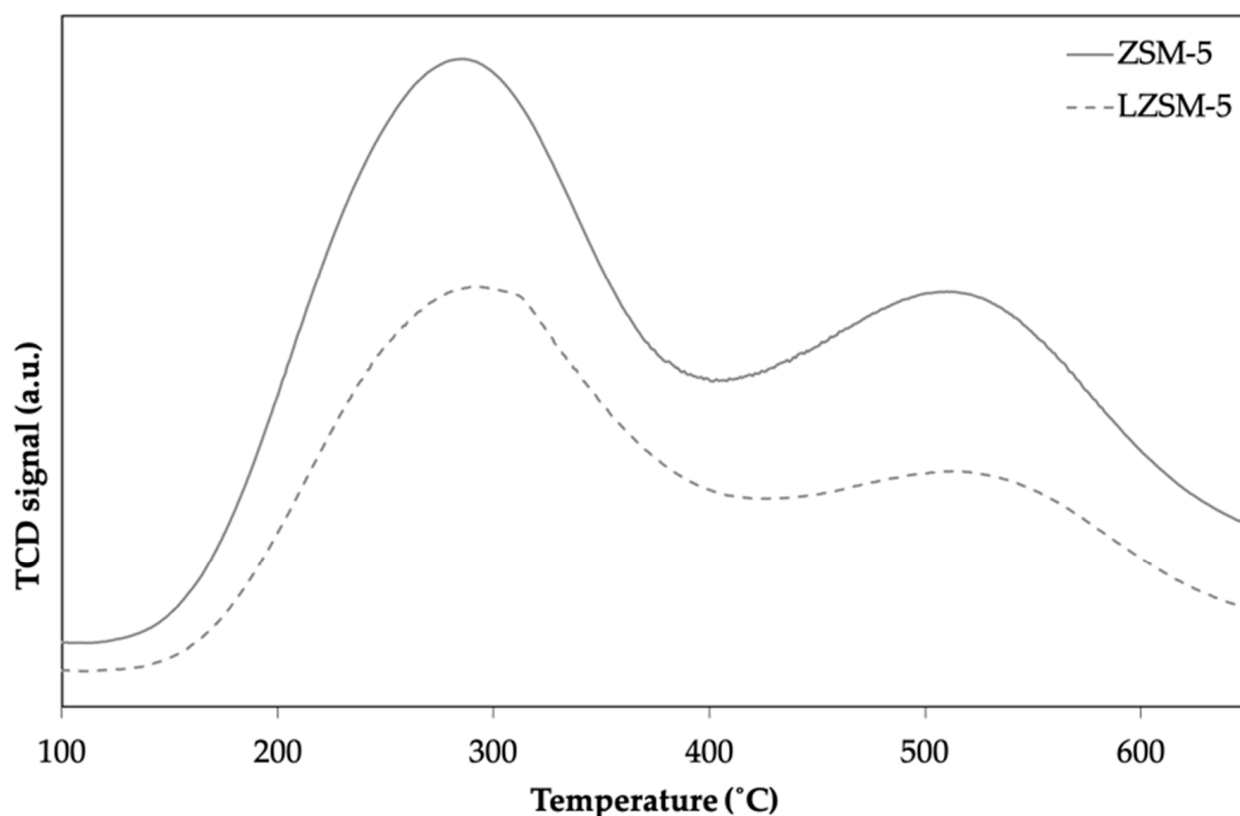


Figure 6. NH₃-TPD profiles for ZSM-5 and LZSM-5 synthesized at 20 h.

Table 2. Total, weak, and strong acidities determined through integration of the peak areas in NH₃-TPD profiles for ZSM-5 and LZSM-5 synthesized at 20 h and their Si/Al ratio determined by EDX.

| Sample | Si/Al | Acidity (mmol g ⁻¹) | | |
|-----------|-------|---------------------------------|------|--------|
| | | Total | Weak | Strong |
| 20-ZSM-5 | 24 | 3.14 | 2.44 | 0.70 |
| 20-LZSM-5 | 28 | 1.07 | 0.96 | 0.11 |

The total acidity of ZSM-5 was 3.14 mmol NH₃ g⁻¹, 78% corresponding to weak acid sites and 22% to strong acid sites. The total acidity of LZSM-5 was 1.07 mmol NH₃ g⁻¹, with 90% of them corresponding to weak acid sites and 10% to strong acid sites. This difference in acid strength might be linked to a peculiar distribution of Al atoms in the zeolite structure due to the introduction of lignin. Considering that the Si/Al ratio remained almost the same for ZSM-5 and LZSM-5, the distribution of framework aluminum determined the acidity, which governs catalyst activity.

3. State and Role of Lignin

There are different physical and chemical methods for lignin characterization. Nevertheless, NMR spectroscopy remains the most reliable for understanding lignin structure. Thus, lignin was analyzed using ¹H liquid NMR (in D₂O) to determine the molecules present in the alkaline hydrolysate during ZSM-5 synthesis. These results can be seen in the ¹H spectrum (Figure 7).

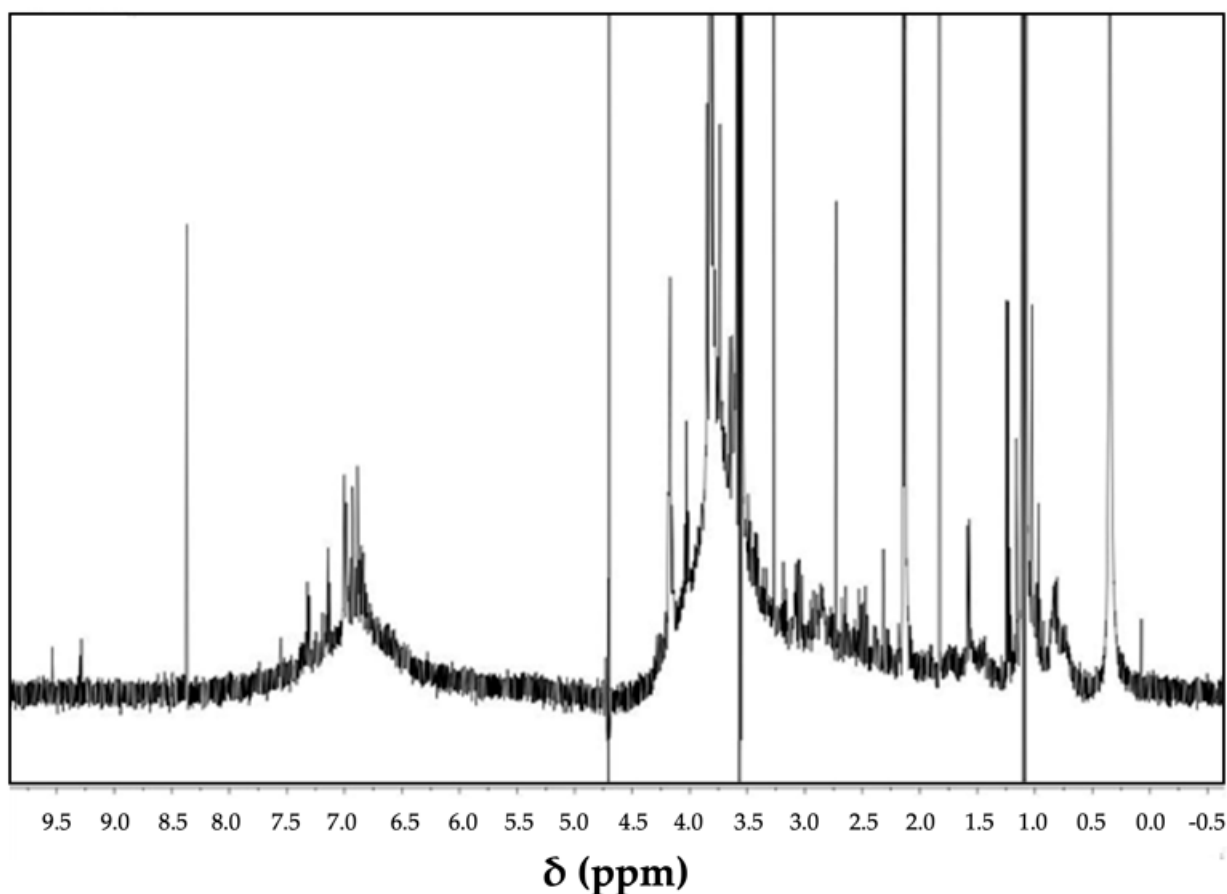


Figure 7. $^1\text{H-NMR}$ spectrum of alkaline hydrolysate of lignin in D_2O .

The assignment of chemical shifts in the region between $\delta = 6.0$ and 8.0 ppm suggests the presence of aromatic -OH^- hydrons from syringyl (S) and guaiacyl (G) units, while the signals between 4.2 and 5.5 ppm could be attributed to aliphatic hydrons ($\text{H}\alpha$ and $\text{H}\beta$) [57,58]. The intense signal of the methoxy group shifted from 3.75 to 3.67 ppm. This group establishes a proportion between S and G. The signal range from 0.25 to 2.9 ppm might be linked to aliphatic and acetyl groups [58,59]. The presence of a large number of hydroxyl groups in the lignocellulosic material likely worked as interactive sites with the zeolite precursors, according to Zou and co-workers [36,37].

The TGA and NMR results confirmed that lignin plays a role in the zeolite crystal assembly. Generally, the alkaline environment during zeolite synthesis first causes phenolic OH^- deprotonation from lignin, giving rise to methoxy groups [59]. This suggests that methyl groups could be linked to silicon and aluminum atoms by oxygen bridges, similar to OH^- bridging [29]. Therefore, methoxy groups may be available to interact with oxygen atoms linked to silicon and aluminum atoms. The mechanism by which zeolite assembly occurs with either cation or methoxy groups remains unknown and, therefore, requires in-depth NMR and DFT analyses.

4. Catalyst Evaluation

In order to better understand the difference between the catalysts obtained with and without lignin, the catalysts were tested in the methanol-to-hydrocarbons (MTH) reaction. The results for MTH catalytic evaluation are shown in Table 3. Methanol conversion ranged between 50 and 100% for ZSM-5 and between 61 and 100% for LZSM-5. $\text{C}_2 = \text{C}_4$ selectivity was higher for the catalysts synthesized using only TPAOH, in particular, 24-ZSM-5 and 20-ZSM-5; meanwhile, catalysts synthesized using both TPAOH and lignin directed the reaction toward DME formation.

Table 3. Methanol conversion and hydrocarbon selectivity achieved over as-synthesized catalysts during the MTH reaction.

| Catalyst | Conversion (%) | Selectivity (%) | | | | | | k_d (h^{-1}) |
|-----------|----------------|-----------------|---------------------------------|----------------|------------------|-----|-----------------|-----------------------|
| | | C ₁ | C ₂ = C ₄ | C ₃ | i-C ₄ | DME | C ₅₊ | |
| 12-ZSM-5 | 65 | - | 4 | 3 | - | 91 | 2 | 0.161 |
| 12-LZSM-5 | 57 | - | 7 | 7 | - | 85 | 1 | 0.205 |
| 16-ZSM-5 | 50 | - | 29 | 26 | - | 20 | 25 | 0.020 |
| 16-LZSM-5 | 61 | - | 3 | 4 | - | 92 | 1 | 0.013 |
| 20-ZSM-5 | 100 | - | 31 | 25 | 13 | 1 | 29 | 0.026 |
| 20-LZSM-5 | 81 | - | 18 | 10 | - | 68 | 4 | 0.287 |
| 24-ZSM-5 | 100 | 2 | 44 | 46 | 3 | - | 5 | * |
| 24-LZSM-5 | 100 | - | 31 | 25 | 12 | 16 | 17 | * |

* Conversion 100% does not present deactivation coefficient (k_d).

The relatively high selectivity toward light olefins for ZSM-5 (higher than 55%) also causes secondary reactions over acid catalysts. Considering the hydrocarbon pool mechanism (HCP) proposed by Dahl and Kolbe, cyclic organic species confined within the pores can act as co-catalysts for the production of olefins from methanol [60,61]. Likewise, ZSM-5 has high crystallinity (over 85%) and stronger acid sites (around 7 times stronger than LZSM-5) while having the same surface area ($\sim 350 \text{ m}^2 \text{ g}^{-1}$) as LZSM-5. This also explains the selectivity of ZSM-5 toward light olefins and hydrocarbons with respect to DME.

Regarding the catalysts synthesized using lignin, 24-LZSM-5 showed the highest olefin selectivity (31%) compared to the other LZSM-5 catalysts. On the other hand, these catalysts exhibited higher DME selectivity (at least 60%). The difference in the MTH catalytic performance for LZSM-5 was likely due to the difference in their acidity and morphological structure, induced by lignin introduction. The path from methanol toward DME consists of dehydration over acid sites and does not require strong acidity. The higher DME selectivity for LZSM-5 might also correlate to the fact that 90% of the latter zeolite acid sites are weak.

Table 3 also shows the deactivation coefficient of each catalyst. In general, the catalysts with lignin led to a faster deactivation than that of the ZSM-5 catalysts. The catalysts synthesized for 24 h did not exhibit a deactivation coefficient. Nonetheless, DME was formed over 24-LZSM-5, which some authors consider to be the first sign of catalyst deactivation during MTH.

5. Materials and Methods

ZSM-5 Zeolite Synthesis

ZSM-5 zeolite was synthesized using a synthesis gel with an initial composition of 1 NaAlO₂: 3 TPAOH: 13 NaCl: 28 TEOS: 3683 H₂O. Sodium chloride (0.380 g, Sigma-Aldrich, Saint Louis, MO, USA), tetrapropylammonium hydroxide (3.0 g, Sigma-Aldrich, 1 M in H₂O), sodium aluminate (0.040 g, Sigma-Aldrich), and distilled water were mixed until a clear solution was obtained. Then, tetraethyl-orthosilicate (TEOS, 2.8 g, Sigma-Aldrich, 99%) and kraft lignin (0.6 g, Borregaard, Norway) were added to the previous solution. The lignin containing 6.0 at% S, 38.3 at% C, and 4.1 at% H was not pretreated prior to use. The synthesis gel was aged for 90 min at room temperature under vigorous stirring. Afterward, the gel was placed inside a Teflon-lined autoclave (40 mL), and the synthesis was performed under static conditions at 170 °C for 4, 8, 12, 16, 20, or 24 h. After cooling down, the solid was recovered by filtration and washed until a neutral pH was reached. The final solid was calcined at 600 °C for 4 h (5 °C min⁻¹ heating rate) under air to remove organics.

To obtain zeolite in acidic form, two successive exchange steps using 2 M NH₄NO₃ aqueous solution at 80 °C for 1 h (1 g of zeolite per 50 mL) were performed. The ammonium form was finally converted into the protonic form by calcination at 450 °C for 4 h (5 °C min⁻¹ heating rate) under air. The samples were denoted as x-ZSM-5 and x-LZSM-5

for zeolites synthesized using TPAOH and lignin, respectively, where x represents the synthesis duration ($x = 4, 6, 10, 12, 16, 20, \text{ or } 24$).

6. Catalyst Characterization

The samples were characterized by powder X-ray diffraction (XRD) using a Bruker D8 Advance diffractometer equipped with an energy dispersive detector using a monochromatic Cu-K α radiation source. The samples were analyzed using a step of 0.02° and an acquisition time of 0.5 s. The crystallinity of each sample was estimated using New Eva software with the following equations:

$$\%Amorphous = \frac{Global\ area - Reduced\ Area}{Global\ Area} * 100$$

$$\%Crystallinity = 100 - \%Amorphous$$

where the background should be adjusted. The relative crystallinity was calculated based on the ZSM-5 sample with the highest crystallinity (24-ZSM-5) as a reference.

The textural properties of the samples were determined by N₂ adsorption–desorption isotherms on Micromeritics ASAP 2420 apparatus at -196°C . Before the analysis, the samples were degassed under vacuum ($10\ \mu\text{mHg}$) for 1 h at 90°C and then for 4 h at 350°C . The total pore volume (V_{tot}) was calculated from the amount of gas adsorbed at a relative pressure P/P_0 of 0.99. The specific surface area (S_{BET}) was calculated using the BET method; the micropore volume (V_{micro}) was calculated using the t-plot method; and the mesoporous volume (V_{meso}) was calculated by the difference between V_{tot} and V_{micro} .

The morphology of the as-prepared samples was observed using scanning electron microscopy (SEM). A Zeiss electronic microscope working at a 9 kV accelerating voltage was used. Prior to the analysis, the samples were placed on aluminum brackets with carbon tape and metalized with gold.

Thermogravimetric analysis (TGA) was carried out for zeolites 24-ZSM-5 and 24-LZSM-5 before the calcination step to quantify the weight loss and their domain due to the decomposition of organics. The analysis was performed using a thermobalance Q500 TA Instrument. Around 20 mg of sample was placed inside ceramic crucibles and heated from 25 to 800°C ($50^\circ\text{C}\ \text{min}^{-1}$ heating rate) in air ($25\ \text{mL}\ \text{min}^{-1}$ flux) and an N₂ ($10\ \text{mL}\ \text{min}^{-1}$ flux) atmosphere. During the heating, the weight of the sample and the furnace temperature were recorded until a constant weight was achieved.

The acidic properties of two catalysts (20-ZSM-5 and 20-LZSM-5) were evaluated by temperature-programmed ammonia desorption (NH₃-TPD) using a Micromeritics AutoChem II chemisorption analyzer equipped with a TCD detector. In all the experiments, 100 mg of sample was outgassed in situ at 550°C for 1 h in a He atmosphere. After that, samples were cooled down to room temperature, and 2% NH₃ in He was flown through the reactor. Once physisorbed ammonia was removed, the temperature was gradually enhanced to 700°C .

To better understand the role of lignin in zeolite synthesis, an alkaline hydrolysate of lignin was prepared at the same pH as the zeolite synthesis and analyzed using liquid nuclear magnetic resonance (¹H NMR). A total of 300 mg of lignin was dissolved in NaOH solution following the same pH and conditions used to synthesize 24-ZSM-5. Around 40 mg of this solution was weighed, and 0.6 mg of D₂O was added. NMR experiments were conducted on a Bruker Avance III HD 500 MHz spectrometer equipped with a 5 mm BBFO cryoprobe and operating at 500.24 MHz for ¹H and 125.80 MHz for ¹³C. Pulse sequences were taken from the Bruker Library, and experiments were performed at 25°C .

7. Catalytic Tests

Methanol-to-hydrocarbon (MTH) reaction experiments were performed in a quartz tubular fixed-bed reactor. The catalyst was packed between two quartz wool plugs. Prior to testing, 60 mg zeolites were activated in situ using argon gas flow ($20\ \text{mL}\ \text{min}^{-1}$) at 550°C

for 1 h. After the reactor was cooled down to 450 °C, the flow was switched to methanol under atmospheric pressure. The flow was adjusted to obtain a weight hourly space velocity (WHSV) of 2 g_{MeOH} g_{catalyst}⁻¹ h⁻¹. The activity of the samples was expressed in terms of converted methanol [27]. The products at the reactor outlet were collected every 30 min for 3 h and analyzed in a gas chromatographer equipped with a 50 m capillary column (PONA) and a flame ionization detector (FID). Methanol conversion and the selectivity toward different hydrocarbons were calculated according to the following formula:

$$\%Conversion_{MeOH} = \frac{(n_{MeOH}^i - n_{MeOH}^o)}{n_{MeOH}^i} \times 100$$

$$\%Selectivity_y = \frac{(\sum n_y^o)}{\%Conversion_{MeOH}} \times 100$$

where n^i and n^o are the moles of the component at the inlet and the outlet of the reactor, respectively; y refers to the hydrocarbon products (C₁, C₂ = C₄, C₃, C₄, DME, and C₅₊).

Catalyst deactivation rates were compared using the activity function defined as

$$X = X_0 * \exp(-k_d * t)$$

where X and X_0 are the methanol conversion, t is the time on stream (TOS), and k_d is the deactivation coefficient. The deactivation rates calculated for the catalysts followed zero-order linear kinetics.

8. Conclusions

ZSM-5 zeolites were successfully prepared in the presence of lignin during hydrothermal synthesis. We demonstrated that it is possible to replace 50% of TPAOH with lignin. The high concentration of functional groups in lignin, such as hydroxyl and methoxy, interacted with aluminosilicate species during zeolite synthesis. This impacted the zeolite self-assembly mechanism. Similarly, different crystallization behavior led to French-fries aggregated in spherical shapes and a different amount of acid sites. The catalyst in the presence of lignin had varying activity and selectivity in MTH. ZSM-5 synthesized with only TPAOH led to olefins, whilst ZSM-5 synthesized with lignin showed higher selectivity toward DME. These changes may be linked to crystal morphology and the distribution of the acid sites on the catalysts.

Supplementary Materials: The following supporting information can be downloaded at: <https://www.mdpi.com/article/10.3390/catal12040368/s1>, Figure S1: Nitrogen adsorption isotherm for 4-ZSM-5, a zeolite synthesized with TPAOH for a duration of 4 h. Figure S2: Nitrogen adsorption isotherms for zeolites synthesized with TPAOH (ZSM-5) for durations of 8, 12, 16, 20, and 24 h. Figure S3: Nitrogen adsorption isotherms for zeolites synthesized with TPAOH and lignin (LZSM-5) for durations of 4, 8, 12, 16, 20, and 24 h.

Author Contributions: All authors contributed extensively to the work presented in this paper. C.G.F. designed and performed the zeolite syntheses and catalytic experiments. Data interpretations were made by C.G.F., H.S. and B.L., who wrote the manuscript. All authors have read and agreed to the published version of the manuscript.

Funding: This research received no external funding.

Acknowledgments: The technical assistance from T. Romero and T. Dintzer (ICPEES), and B. Vincent (Faculté de Chimie) was highly appreciated and helped the development of the work.

Conflicts of Interest: The authors declare no conflict of interest.

References

1. Luo, Y.; Funke, H.H.; Falconer, J.L.; Noble, R.D. Adsorption of CO₂, CH₄, C₃H₈, and H₂O in SSZ-13, SAPO-34, and T-Type Zeolites. *Ind. Eng. Chem. Res.* **2016**, *55*, 9749–9757. [[CrossRef](#)]
2. Megías-Sayago, C.; Bingre, R.; Huang, L.; Lutzweiler, G.; Wang, Q.; Louis, B. CO₂ Adsorption Capacities in Zeolites and Layered Double Hydroxide Materials. *Front. Chem.* **2019**, *7*, 551. [[CrossRef](#)]
3. Demirci, S.; Ustaoglu, Z.; Yilmazer, G.A.; Sahin, F.; Baç, N. Antimicrobial Properties of Zeolite-X and Zeolite-A Ion-Exchanged with Silver, Copper, and Zinc against a Broad Range of Microorganisms. *Appl. Biochem. Biotechnol.* **2014**, *172*, 1652–1662. [[CrossRef](#)] [[PubMed](#)]
4. Flores, C.G.; Schneider, H.; Ferret, L.; Marcilio, N.R.; Oliveira, J.C.P. Potassic Zeolites from Brazilian Coal Ash for Use as a Fertilizer in Agriculture. *Waste Manag.* **2017**, *70*, 263–271. [[CrossRef](#)]
5. Li, J.; Zhuang, X.; Font, O.; Moreno, N.; Vallejo, V.R.; Querol, X.; Tobias, A. Synthesis of Merlinoite from Chinese Coal Fly Ashes and Its Potential Utilization as Slow Release K-Fertilizer. *J. Hazard. Mater.* **2014**, *265*, 242–252. [[CrossRef](#)]
6. Pereira, S.C.; Souza, M.; Esteves, L.M.; Batalha, N.; Lam, Y.L.; Pereira, M.M. Hydroconversion of Xylose Derived Ketals: A Key Strategy for Producing A Broad Range of Green-Hydrocarbons Suitable as Fuels and Petrochemicals. *Appl. Catal. A Gen.* **2021**, *609*, 117911. [[CrossRef](#)]
7. Flores, C.; Batalha, N.; Ordonsky, V.V.; Zholobenko, V.L.; Baaziz, W.; Marcilio, N.R.; Khodakov, A.Y. Direct Production of Iso-Paraffins from Syngas over Hierarchical Cobalt-ZSM-5 Nanocomposites Synthesized by Using Carbon Nanotubes as Sacrificial Templates. *ChemCatChem* **2018**, *10*, 2291–2299. [[CrossRef](#)]
8. Flores, C.; Batalha, N.; Marcilio, N.R.; Ordonsky, V.V.; Khodakov, A.Y. Influence of Impregnation and Ion Exchange Sequence on Metal Localization, Acidity and Catalytic Performance of Cobalt BEA Zeolite Catalysts in Fischer-Tropsch Synthesis. *ChemCatChem* **2018**, *11*, 568–574. [[CrossRef](#)]
9. Van Daele, S.; Minoux, D.; Nesterenko, N.; Maury, S.; Coupard, V.; Valtchev, V.; Travert, A.; Gilson, J.P. A Highly Selective FER-Based Catalyst to Produce n-Butenes from Isobutanol. *Appl. Catal. B Environ.* **2021**, *284*, 119699. [[CrossRef](#)]
10. Martínez, C.; Corma, A. Inorganic Molecular Sieves: Preparation, Modification and Industrial Application in Catalytic Processes. *Coord. Chem. Rev.* **2011**, *255*, 1558–1580. [[CrossRef](#)]
11. Primo, A.; Garcia, H. Zeolites as Catalysts in Oil Refining. *Chem. Soc. Rev.* **2014**, *43*, 7548–7561. [[CrossRef](#)]
12. Weitkamp, J. Zeolites and Catalysis. *Solide State Ionics* **2000**, *131*, 175–188. [[CrossRef](#)]
13. Jae, J.; Tompsett, G.A.; Foster, A.J.; Hammond, K.D.; Auerbach, S.M.; Lobo, R.F.; Huber, G.W. Investigation into the Shape Selectivity of Zeolite Catalysts for Biomass Conversion. *J. Catal.* **2011**, *279*, 257–268. [[CrossRef](#)]
14. Mores, D.; Kornatowski, J.; Olsbye, U.; Weckhuysen, B.M. Coke Formation during the Methanol-to-Olefin Conversion: In Situ Microspectroscopy on Individual H-ZSM-5 Crystals with Different Brønsted Acidity. *Chem. A Eur. J.* **2011**, *17*, 2874–2884. [[CrossRef](#)] [[PubMed](#)]
15. Wan, Z.; Wu, W.; Li, G.; Wang, C.; Yang, H.; Zhang, D. Effect of SiO₂/Al₂O₃ Ratio on the Performance of Nanocrystal ZSM-5 Zeolite Catalysts in Methanol to Gasoline Conversion. *Appl. Catal. A Gen.* **2016**, *523*, 312–320. [[CrossRef](#)]
16. Shirazi, L.; Jamshidi, E.; Ghasemi, M.R. The Effect of Si/Al Ratio of ZSM-5 Zeolite on Its Morphology, Acidity and Crystal Size. *Cryst. Res. Technol.* **2008**, *43*, 1300–1306. [[CrossRef](#)]
17. Serrano, D.P.; Escola, J.M.; Pizarro, P. Synthesis Strategies in the Search for Hierarchical Zeolites. *Chem. Soc. Rev.* **2013**, *42*, 4004–4035. [[CrossRef](#)] [[PubMed](#)]
18. Davis, M.E.; Lobo, R.F. Zeolite and Molecular Sieve Synthesis. *Chem. Mater.* **1992**, *4*, 756–768. [[CrossRef](#)]
19. Flanigen, E.M.; Bennett, J.M.; Grose, R.W.; Cohen, J.P.; Patton, R.L.; Kirchner, R.M.; Smith, J.V. Silicalite, a New Hydrophobic Crystalline Silica Molecular Sieve. *Nature* **1978**, *271*, 512–516. [[CrossRef](#)]
20. Burkett, S.L.; Davis, M.E. Mechanism of Structure Direction in the Synthesis of Si-ZSM-5: An Investigation by Intermolecular 1H-29Si CP MAS NMR. *J. Phys. Chem.* **1994**, *98*, 4647–4653. [[CrossRef](#)]
21. Sang, S.; Chang, F.; Liu, Z.; He, C.; He, Y.; Xu, L. Difference of ZSM-5 Zeolites Synthesized with Various Templates. *Catal. Today* **2004**, *93–95*, 729–734. [[CrossRef](#)]
22. Meng, X.; Xiao, F.S. Green Routes for Synthesis of Zeolites. *Chem. Rev.* **2014**, *114*, 1521–1543. [[CrossRef](#)] [[PubMed](#)]
23. Lee, H.; Zones, S.I.; Davis, M.E. A Combustion-Free Methodology for Synthesizing Zeolites and Zeolite-like Materials. *Nature* **2003**, *425*, 385–388. [[CrossRef](#)]
24. Grand, J.; Awala, H.; Mintova, S. Mechanism of Zeolites Crystal Growth: New Findings and Open Questions. *CrystEngComm* **2016**, *18*, 650–664. [[CrossRef](#)]
25. Maldonado, M.; Oleksiak, M.D.; Chinta, S.; Rimer, J.D. Controlling Crystal Polymorphism in Organic-Free Synthesis of Na-Zeolites. *J. Am. Chem. Soc.* **2013**, *135*, 2641–2652. [[CrossRef](#)]
26. Louis, B.; Gomes, E.S.; Losch, P.; Lutzweiler, G.; Coelho, T.; Faro, A.; Pinto, J.F.; Cardoso, C.S.; Silva, A.V.; Pereira, M.M. Biomass-Assisted Zeolite Syntheses as a Tool for Designing New Acid Catalysts. *ChemCatChem* **2017**, *9*, 2065–2079. [[CrossRef](#)]
27. Bingre, R.; Sayago, C.M.; Losch, P.; Huang, L.; Wang, Q.; Pereira, M.M.; Louis, B. Recent Progress in the Biomass-Mediated Synthesis of Porous Materials. *Inorg. Chim. Acta* **2019**, *487*, 379–386. [[CrossRef](#)]
28. Gomes, E.S.; Lutzweiler, G.; Losch, P.; Silva, A.V.; Bernardon, C.; Parkhomenko, K.; Pereira, M.M.; Louis, B. Strategy to Design Zeolite Catalysts in the Presence of Biomass. *Microporous Mesoporous Mater.* **2017**, *254*, 28–36. [[CrossRef](#)]

29. Ocampo, F.; Cunha, J.A.; De Lima Santos, M.R.; Tessonnier, J.P.; Pereira, M.M.; Louis, B. Synthesis of Zeolite Crystals with Unusual Morphology: Application in Acid Catalysis. *Appl. Catal. A Gen.* **2010**, *390*, 102–109. [[CrossRef](#)]
30. Gomes, E.S.; Aranda, D.A.G.; Pereira, M.M.; Louis, B. ZSM-5 Synthesis by the Assistance of Biomass and Biomass-Derivate Compounds. *Microporous Mesoporous Mater.* **2018**, *263*, 251–256. [[CrossRef](#)]
31. Silva, A.V.; Miranda, L.S.M.; Nele, M.; Louis, B.; Pereira, M.M. Insights to Achieve a Better Control of Silicon-Aluminum Ratio and ZSM-5 Zeolite Crystal Morphology through the Assistance of Biomass. *Catalysts* **2016**, *6*, 30. [[CrossRef](#)]
32. Ali, I.O.; Thabet, M.S.; El-Nasser, K.S.; Hassan, A.M.; Salama, T.M. Synthesis of Nanosized ZSM-5 Zeolite from Rice Straw Using Lignin as a Template: Surface-Modified Zeolite with Quaternary Ammonium Cation for Removal of Chromium from Aqueous Solution. *Microporous Mesoporous Mater.* **2012**, *160*, 97–105. [[CrossRef](#)]
33. Mintova, S.; Barrier, N. *Verified Syntheses of Zeolitic Materials*, 3rd ed.; Synthesis Commission of the International Zeolite Association: Amsterdam, The Netherlands, 2016; ISBN 9780692685396.
34. Burton, A.W.; Zones, S.I. Chapter 5: Organic Molecules in Zeolite Synthesis: Their Preparation and Structure-Directing Effects. *Stud. Surf. Sci. Catal.* **2007**, *68*, 137–179.
35. Peter, A.; Jacobs, J.A.M. Synthesis of ZSM-5 Zeolites in the Presence of Tetrapropylammonium Ions. *Stud. Surf. Sci. Catal.* **1987**, *33*, 47–111.
36. Qian, M.; Lei, H.; Zhao, Y.; Villota, E.; Huo, E.; Wang, C.; Zhang, X. Lignin-Mediated Preparation of Hierarchical ZSM-5 Catalysts and Their Effects in the Catalytic Co-Pyrolysis of Softwood Biomass and Low-Density Polyethylene Mixtures. *ACS Sustain. Chem. Eng.* **2021**, *9*, 12602–12613. [[CrossRef](#)]
37. Qian, M.; Lei, H.; Villota, E.; Zhao, Y.; Huo, E.; Wang, C.; Mateo, W.; Zou, R. Enhanced Production of Renewable Aromatic Hydrocarbons for Jet-Fuel from Softwood Biomass and Plastic Waste Using Hierarchical ZSM-5 Modified with Lignin-Assisted Re-Assembly. *Energy Convers. Manag.* **2021**, *236*, 114020. [[CrossRef](#)]
38. Van Grieken, R.; Sotelo, J.L.; Menendez, J.M.; Melero, J.A. Anomalous Crystallization Mechanism in the Synthesis of Nanocrystalline ZSM-5. *Microporous Mesoporous Mater.* **2000**, *39*, 135–147. [[CrossRef](#)]
39. Pereira, M.M.; Gomes, E.S.; Silva, A.V.; Pinar, A.B.; Willinger, M.G.; Shanmugam, S.; Chizallet, C.; Laugel, G.; Losch, P.; Louis, B. Biomass-Mediated ZSM-5 Zeolite Synthesis: When Self-Assembly Allows to Cross the Si/Al Lower Limit. *Chem. Sci.* **2018**, *9*, 6532–6539. [[CrossRef](#)]
40. Alipour, S.M.; Halladj, R.; Askari, S. Effects of the Different Synthetic Parameters on the Crystallinity and Crystal Size of Nanosized ZSM-5 Zeolite. *Rev. Chem. Eng.* **2014**, *30*, 289–322. [[CrossRef](#)]
41. Mohamed, R.M.; Fouad, O.A.; Ismail, A.A.; Ibrahim, I.A. Influence of Crystallization Times on the Synthesis of Nanosized ZSM-5. *Mater. Lett.* **2005**, *59*, 3441–3444. [[CrossRef](#)]
42. Thommes, M.; Kaneko, K.; Neimark, A.V.; Olivier, J.P.; Rodriguez-Reinoso, F.; Rouquerol, J.; Sing, K.S.W. Physisorption of Gases, with Special Reference to the Evaluation of Surface Area and Pore Size Distribution (IUPAC Technical Report). *Pure Appl. Chem.* **2015**, *87*, 1051–1069. [[CrossRef](#)]
43. Humphreys, J.M.; Chapple, C. Rewriting the Lignin Roadmap. *Curr. Opin. Plant Biol.* **2002**, *5*, 224–229. [[CrossRef](#)]
44. Serrano, D.P.; Pinnavaia, T.J.; Aguado, J.; Escola, J.M.; Peral, A.; Villalba, L. Hierarchical ZSM-5 Zeolites Synthesized by Silanization of Protozeolitic Units: Mediating the Mesoporosity Contribution by Changing the Organosilane Type. *Catal. Today* **2003**, *227*, 15–25. [[CrossRef](#)]
45. Serrano, D.P.; Aguado, J.; Escola, J.M.; Peral, A.; Morales, G.; Abella, E. Synthesis of Hierarchical ZSM-5 by Silanization and Alkoxylation of Protozeolitic Units. *Catal. Today* **2011**, *168*, 86–95. [[CrossRef](#)]
46. Wang, Y.; Ma, J.; Ren, F.; Du, J.; Li, R. Hierarchical Architectures of ZSM-5 Nanocrystalline Aggregates with Particular Catalysis for Lager Molecule Reaction. *Microporous Mesoporous Mater.* **2017**, *240*, 22–30. [[CrossRef](#)]
47. Parker, L.M.; Bibby, D.M.; Patterson, J.E. Thermal Decomposition of ZSM-5 and Silicalite Precursors. *Zeolites* **1984**, *4*, 168–174. [[CrossRef](#)]
48. Ház, A.; Jablonský, M.; Šurina, I.; Kačík, F.; Bubeníková, T.; Ďurkovič, J. Chemical Composition and Thermal Behavior of Kraft Lignins. *Forests* **2019**, *10*, 483. [[CrossRef](#)]
49. El Moustaqim, M.; El Kaihal, A.; El Marouani, M.; Men-La-Yakhaf, S.; Taibi, M.; Sebbahi, S.; El Hajjaji, S.; Kifani-Sahban, F. Thermal and Thermomechanical Analyses of Lignin. *Sustain. Chem. Pharm.* **2018**, *9*, 63–68. [[CrossRef](#)]
50. Zhao, J.; Xiuwen, W.; Hu, J.; Liu, Q.; Shen, D.; Xiao, R. Thermal Degradation of Softwood Lignin and Hardwood Lignin by TG-FTIR and Py-GC/MS. *Polym. Degrad. Stab.* **2014**, *108*, 133–138. [[CrossRef](#)]
51. Hsu, C.Y.; Chiang, A.S.T.; Selvin, R.; Thompson, R.W. Rapid Synthesis of MFI Zeolite Nanocrystals. *J. Phys. Chem. B* **2005**, *109*, 18804–18814. [[CrossRef](#)]
52. Watkins, D.; Nuruddin, M.; Hosur, M.; Tcherbi-Narteh, A.; Jeelani, S. Extraction and Characterization of Lignin from Different Biomass Resources. *J. Mater. Res. Technol.* **2015**, *4*, 26–32. [[CrossRef](#)]
53. Katada, N.; Igi, H.; Kim, J.H.; Niwa, M. Determination of the Acidic Properties of Zeolite by Theoretical Analysis of Temperature-Programmed Desorption of Ammonia Based on Adsorption Equilibrium. *J. Phys. Chem. B* **1997**, *101*, 5969–5977. [[CrossRef](#)]
54. Sato, H. Acidity Control and Catalysis of Pentasil Zeolites. *Catal. Rev.* **1997**, *39*, 395–424. [[CrossRef](#)]
55. Zhang, Q.; Yang, H.; Yan, W. Effect of Ethanol on the Crystallinity and Acid Sites of MFI Zeolite Nanosheets. *RSC Adv.* **2014**, *4*, 56938–56944. [[CrossRef](#)]

56. Lónyi, F.; Valyon, J. On the interpretation of the NH₃-TPD patterns of H-ZSM-5 and H-mordenite. *Microporous Mesoporous Mater.* **2001**, *47*, 293–301. [[CrossRef](#)]
57. Lu, Y.; Lu, Y.C.; Hu, H.Q.; Xie, F.J.; Wei, X.Y.; Fan, X. Structural Characterization of Lignin and Its Degradation Products with Spectroscopic Methods. *J. Spectrosc.* **2017**, *2017*, 8951658. [[CrossRef](#)]
58. García, A.; Toledano, A.; Serrano, L.; Egüés, I.; González, M.; Marín, F.; Labidi, J. Characterization of Lignins Obtained by Selective Precipitation. *Sep. Purif. Technol.* **2009**, *68*, 193–198. [[CrossRef](#)]
59. Diop, A.; Jradi, K.; Daneault, C.; Montplaisir, D. Kraft Lignin Depolymerization in an Ionic Liquid without a Catalyst. *BioResources* **2015**, *10*, 4933–4946. [[CrossRef](#)]
60. Modenbach, A.A. Effects of Sodium Hydroxide Pretreatment on Structural Components of Biomass. *Biosyst. Agricultural Eng.* **2014**, *57*, 1187–1198. [[CrossRef](#)]
61. Dahl, I.M.; Kolboe, S. On the Reaction Mechanism for Hydrocarbon Formation from Methanol over SAPO-34. I. Isotopic Labeling Studies of the Co-Reaction of Ethene and Methanol. *J. Catal.* **1994**, *149*, 458–464. [[CrossRef](#)]